ACS APPLIED OPTICAL MATERIALS

pubs.acs.org/acsaom

Forum Article

Compact Foveated AR Displays with Polarization Selective Planar Lenses

Qian Yang, Yannanqi Li, Yuqiang Ding, and Shin-Tson Wu*

Cite This: https://doi.org/10.1021/acsaom.2c00203

Read Online

ACCESS | Metrics & More | Article Recommendations | Supporting Information

ABSTRACT: The rapid development of powerful microprocessors, high-pixel density display panels, thin and small formfactor optics, and precise device fabrication capabilities enable wearable near-eye displays for augmented reality (AR) and virtual reality (VR) applications. However, in traditional near-eye displays, there is often a trade-off between field of view (FoV) and angular resolution when a single microdisplay light engine is employed. A high-resolution display panel helps overcome this conflict, but the device fabrication remains a challenge, not to mention the issues like huge data transfer, circuit overheating, and high computational load. Here, we propose a Maxwellian-type foveated AR display based on a single microdisplay light engine by using a temporal polarization multiplexing method, enabled by two polarization selective flat cholesteric liquid crystal lenses. One polarization lens provides a large FoV while the other realizes a high angular resolution imaging in a small fovea region. Moreover, the vergence-accommodation conflict issue is inherently nonexistent in the Maxwellian display, and the aberration can be eliminated for each view by matching the recording and reconstructing signals. In an experiment, we constructed a display breadboard and demonstrated that the angular resolution of the foveal view is enhanced by 3.12× while maintaining a compact formfactor. This work paves the way for implementing high-performance foveated AR displays while keeping a compact formfactor.

KEYWORDS: *foveated display, Maxwellian display, flat lenses, temporal and polarization multiplexing*

INTRODUCTION

Thanks to the rapid development of powerful microprocessors, high-pixel density display panels, thin and small formfactor optics, and precise device fabrication capabilities, near-eye displays (NEDs) have finally come into our lives. Both virtual reality (VR) and augmented reality (AR) can enhance our perception and interaction with the real world.[1,2] While VR generates a fully immersive, artificial environment for the user to engage with, AR blends digital elements with the user's see-through surroundings. Despite the release of several commercial AR headsets, such as Google Glass, Microsoft HoloLens, and Magic Leap 2, the challenge remains in delivering high-quality images in a compact size that meets consumer's expectations. The design of such devices should fit the human vision system (HVS)[3] and be compact and lightweight for a comfortable long-term wearing, while minimizing visual fatigue caused by the vergence-accommodation conflict (VAC).[4−6] Since the binocular overlapping field of view (FoV) in HVS is more than 100° and the highest visual acuity is about 30 cycles per degree (cpd, or 60 pixels per degree), the NED should cover a wide FoV while satisfying high angular resolution. However, in a traditional NED, there is often a trade-off between FoV and angular resolution for a single microdisplay light engine. Commercial products often prioritize wide FoV over high angular resolution, resulting in an annoying screen-door effect. One potential solution is to use a high-resolution panel as the light engine, but to achieve human visual acuity a 6 K display panel is required for the 100° FoV. Although it is possible to fabricate such a high pixel-density panel (>3000 pixels per inch), the production yield, high frame rate (say, 120 Hz), large amount of data transfer, thermal effect, high computational load, and high power consumption remain technical challenges.

Noticing that the human visual acuity decreases rapidly away from the fovea, the whole FoV can be divided into foveal and peripheral regions, and each part can be rendered in different resolution. The perceived resolution varies across the image, where the foveal region requires a higher pixel density than the peripheral. Foveated displays are conceived based on this characteristic of the HVS. In this way, the huge pixel number requirement and rendering burden is greatly relieved while providing an overall immersive experience to the user. For example, Tan et al. proposed a dual-resolution VR system utilizing two display panels with different optical magnification, where the foveated region shifting is achieved by a switchable liquid crystal (LC) deflector.[7] Kim et al. built an AR system where the foveated region is steered by moving the microdisplay, and the eyebox of the Maxwellian peripheral view is expanded by translating the holographic optical element.[8] Lee et al. implemented a two-display-module AR display by combining a holographic foveal display and a peripheral display based on polarization volume lenses and diffusers.[9]

Special Issue: Optical Materials and Applications for AR and VR Display Systems

Received: December 29, 2022
Accepted: February 15, 2023

Yet, the two employed light engines inevitably take up valuable space in an NED, especially for an eyeglasses-like AR display. Efforts have been made to realize an optically foveated display in a single light engine. Lyu et al. proposed a perceptual-driven approach for designing a statically foveated NED with a wide FoV and minimal image degradation.[10] Yoo et al. designed a VR system including two doublets based on Pancharatnam−Berry phase lenses (PBLs), where the light from the same display panel experiences different optical power according to its polarization state.[11] Similarly, Yin et al. demonstrated a pancake-like foveated VR system with an impressive 4.4× enhancement ratio.[12]

In this paper, we propose a Maxwellian-type foveated AR system using a single light engine. The high-resolution foveal image and the low-resolution peripheral image are encoded into the light engine by a temporal polarization-multiplexing method. Two polarization-sensitive off-axis cholesteric liquid crystal (CLC) lenses and a PBL are employed to separate the two views. One polarization provides a large FoV while the other realizes a high angular resolution imaging in a small fovea region. Apart from that, the VAC issue does not exist in Maxwellian displays, and the aberration can be eliminated for each view by matching the recording and reconstruction signals.[13] The proposed architecture effectively reduces the system volume by employing a single display module and achieves a wide FoV and high perceived angular resolution simultaneously.

METHODS

When a chiral compound is doped into a nematic host, the LC will spontaneously form a helical structure. Within a helical pitch, the CLC directors are reoriented from 0 to 2π. The analysis of LC elastic free energy density reveals that the helical structure with a pitch length P leads to a minimal energy state. Thus, photonic devices based on the helical structure of CLC can be achieved through a self-organizing process. According to the helical twist, CLCs can be classified as right-handed CLCs (R-CLC) and left-handed CLCs (L-CLC). If the incident circularly polarized light has the same handness as the helical twist in the planar CLC, at normal incidence, the light propagating along the helix will experience Bragg reflection, while the opposite handedness component will mostly pass through the CLC layer. The reflection band spans over a spectral range of $n_oP < \lambda < n_eP$, where n_o and n_e are the ordinary and extraordinary refractive indices, respectively. By combining CLCs with a patterned alignment layer, photonic devices with arbitrary phase profiles can be created.[14,15] For example, an on-axis CLC lens[16,17] is enabled by adopting a parabolic phase profile, and a large-angle diffraction grating is realized by a sawtooth phase profile.[18−20] The large-scale production of CLC photonic devices can be achieved by the holo-imprinting technique,[21,22] empowering cost-effective fabrication. The CLC devices are particularly attractive for AR applications because ∼50% of the ambient light with an opposite handedness can pass through.[23,24] More importantly, CLC devices can be stacked together to achieve different functions by the polarization-multiplexing method. As illustrated in Figure 1, two CLC lenses with orthogonal handedness are stacked into a polarization selective lens (PSL). When an unpolarized beam hits the PSL, the right-handed circularly polarized (RCP) light converges to a farther spot on the left side while the left-handed circularly polarized (LCP) light converges to a nearer focus point on the right side. The

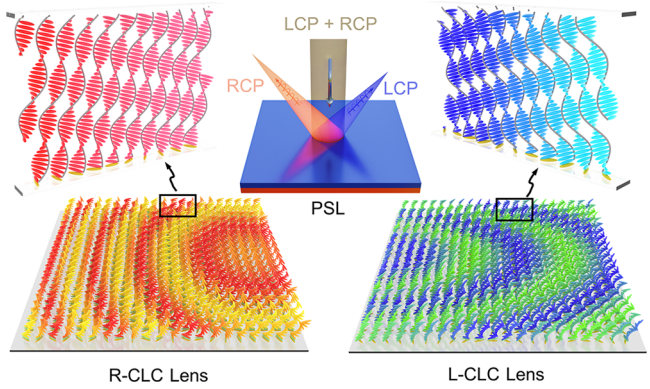

Figure 1. Functionality of a PSL and its microscopic structure. The PSL consists of two CLC lenses with opposite handedness. When an unpolarized beam hits the PSL, the RCP light converges to a farther spot on the left side while the LCP light converges to a nearer focal point on the right side. The phase profiles of R-CLC and L-CLC lenses can be observed from the molecular arrangement.

phase profiles of R-CLC and L-CLC lenses can be observed from the molecular arrangement. The surface treatment provides CLCs with a spatially varying rotation of the LC optical axis on the substrate. The rotation angle changes continually and forms non-centrosymmetric parabolic phase profiles. When one zooms into a small portion of the LC director structure, the CLCs are twisted along a slanted axis and look like a local polarization volume grating[25,26] whose horizontal periods and slanted angles vary spatially. Meanwhile, the CLC twist direction is opposite in the two lenses, which is the origin of the polarization selectivity.

Figure 2a depicts the system configuration of the proposed Maxwellian-type foveated AR display based on the PSL. The

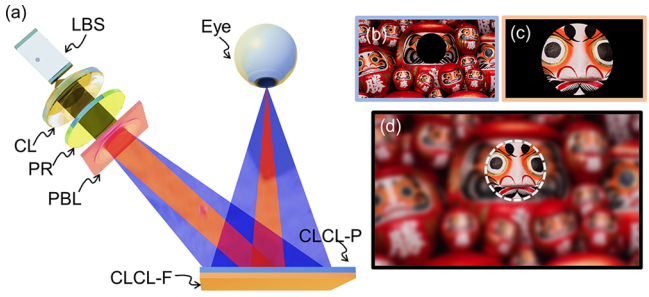

Figure 2. (a) Sketch of a Maxwellian-type foveated AR display. (b) Input image for peripheral view. (c) Input image for foveated view. (d) Simulated perceived image on the retina. The white dashed lines outline the high-resolution part of an image projected on the foveal region of the retina.

PSL consists of two off-axis CLC lenses, functioning as see-through imaging combiners, which are responsible for the foveal and peripheral views, as shown in Figure 2b,c, respectively. By combining the two views, the eye will perceive a complete image like Figure 2d. The CLC lens for the foveal view is denoted as CLCL-F, and the other for the peripheral view is denoted as CLCL-P. The two CLC lenses respond to LCP and RCP lights, respectively. Each lens works in a Maxwellian way and has different effective areas to provide different FoVs, since the FoV is related to the lens area and the distance of eye relief. To ensure all the rays pass through the center of the eye lens, the focal spots of both CLC lenses

https://doi.org/10.1021/acsaom.2c00203
ACS Appl. Opt. Mater. XXXX, XXX, XXX−XXX

should be located at the same point. Assuming the light from the laser beam scanner (LBS) is linearly polarized, it is modulated into a plane-wave-like beam by a collimating lens (CL). The polarization rotator (PR) is composed of a twisted nematic (TN) cell and a quarter-wave plate (QWP) film. By controlling the voltage of the TN cell, the PR can select the desired orthogonal circular polarization state in a time sequence. The RCP and LCP lights behave differently when traversing the PBL, as they encounter opposite phase profiles. For example, the RCP light experiences a positive power and thus is converged, while the LCP light experiences a negative power and is diverged. After passing through the PBL, the handedness is flipped, and the off-axis CLC lenses converge two circularly polarized lights to the center of eye lens, which in turn are projected onto the retina.

A paraxial raytracing analysis of the system can be found in the Supporting Information. The effective diameter (D) of the CLCL-F and the eye relief (ER) jointly determine the foveal FoV (FFoV), as eq 1 indicates. Similarly, peripheral FoV (PFoV) can be traced back from the effective diameter of the CLCL-P (D') by eq 2.

$$D = 2 \times \mathrm{ER} \times \tan\left(\frac{\mathrm{FFoV}}{2}\right) \tag{1}$$

$$\mathrm{PFoV} = 2 \times \arctan\left(\frac{D'}{2 \times \mathrm{ER}}\right) \tag{2}$$

EXPERIMENT

In the initial design, the enhancement ratio is set to be about 3. If we choose FFoV = 17°, PFoV = 54°, and ER = 2.0 cm, then we can deduce that D = 0.6 cm and D' = 2 cm. An off-the-shelf broadband PBL (Edmund Optics) with a focal length of 12 cm at λ = 457 nm is selected. In addition, parameters d, θ, and h are set as 6.5 cm, 45°, and 0.5 cm to meet the design requirement.

A common technique for recording such phase patterns is the photoalignment polarization holography, where the LCP and RCP light beams interfere with each other, projecting a spatially varying linear polarization pattern on the sample. The exposure setup is illustrated in Figure 3a. The beam from the laser (λ = 457 nm, Cobolt Twist) is filtered, expanded, and collimated before it is sent to the polarizing beam splitter (PBS). A half-wave plate is inserted before the PBS to adjust the s and p component ratio of the beam. Two QWPs are employed to realize the LCP and RCP states. A dielectric mirror directs the beam angle in one of optical paths. A PBL and a template lens (TL) are inserted in each optical path to create the designed phase pattern. The exposure setup is built following reciprocity between the reconstruction and recording processes. Figure 3b,c shows the detailed optical path diagrams of CLCL-F and CLCL-P. The TL is a small f-number lens (f/0.8), and its focal length is equal to the ER. The separation between the sample and the TL is twice the ER in Figure 3b,c. The acute angle between two optical axes (red dashed lines) is the complementary angle of θ. The PBL is placed at a distance d from the sample. In Figure 3b, the incident light is RCP. For the exposure setup of CLCL-P, the polarization of incident light is flipped. If the PFoV is set to be symmetric as Figure 3c depicts, then the FFoV will be asymmetric. Noticing that both the mirror and PBL will flip the handedness of a circularly polarized light, the polarization of two beams should be orthogonal after QWP_1 and QWP_2.

The interference pattern is then recorded on the sample substrate coated with a photoalignment layer. First, the substrate is cleaned with ethanol, acetone, and isopropyl alcohol. It is then treated with UV-Ozone for 5 min. The photoalignment material used is Brilliant Yellow, which is supplied by Tokyo Chemical Industry Co., Ltd. The Brilliant Yellow is dissolved in *N*,*N*-dimethylformamide at a concentration of 0.2% by weight and then filtered through a 0.2 μm

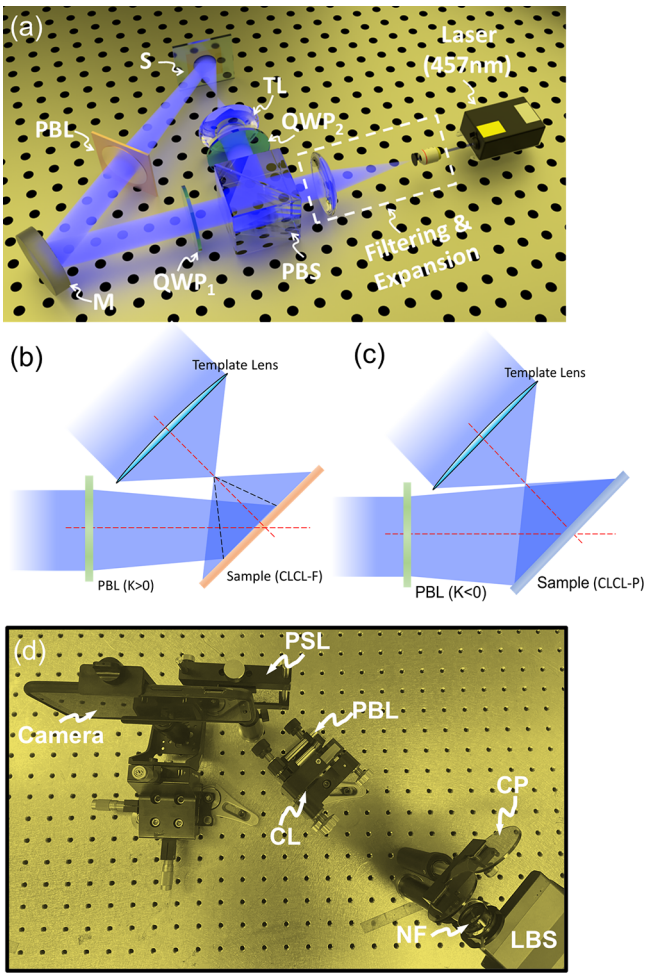

Figure 3. (a) Exposure setup for generating the phase profile for CLC lenses. Detailed optical path diagram of (b) CLCL-F and (c) CLCL-P. (d) The benchtop demonstration of the proposed Maxwellian foveated display. M: dielectric mirror. TL: template lens. S: sample. NF: notch filter at 457 nm. CP: circular polarizer.

Teflon syringe filter to remove impurities. After filtration, the Brilliant Yellow solution is spin-coated onto the substrate. The exposure dosage is about 3 J/cm^2 (35 mW/cm^2 for 1.5 min). Once the exposure is finished, the sample is coated with another layer of CLC mixture. The CLC mixture is made up of 94.28% RM257 (from HCCH), 2.62% chiral dopants R5011 or S5011 (from HCCH), 3% photoinitiator Irgacure 651 (from BASF), and 0.1% surfactant Zonyl 8857A (from Dupont). The composition of R-CLC and L-CLC solvent employed in the lens fabrication is the same except for the handedness of chiral dopants. After that, the CLC mixture is further diluted in toluene at a weight ratio of 1:6, which provides an overall diffraction efficiency of about 60% with the corresponding circularly polarized incident light at λ = 457 nm. The transparency is about 65% with a linearly polarized incident light at 457 nm. The film thickness is about 500 nm measured with a profilometer. The diffraction efficiency is sufficient for an optical combiner in the Maxwellian display. Also, a lower diffraction efficiency is helpful to increase the see-through transmittance after stacking multiple CLC lenses together.

RESULTS AND DISCUSSIONS

The functionality of the CLCL-F is demonstrated in Figure 4a. A collimated beam is modulated by a circular polarizer to obtain a pure RCP light. The light then passes the PBL employed in the exposure process, transforms into a converging beam, and flips its handedness. The zeroth-order

https://doi.org/10.1021/acsaom.2c00203
ACS Appl. Opt. Mater. XXXX, XXX, XXX−XXX

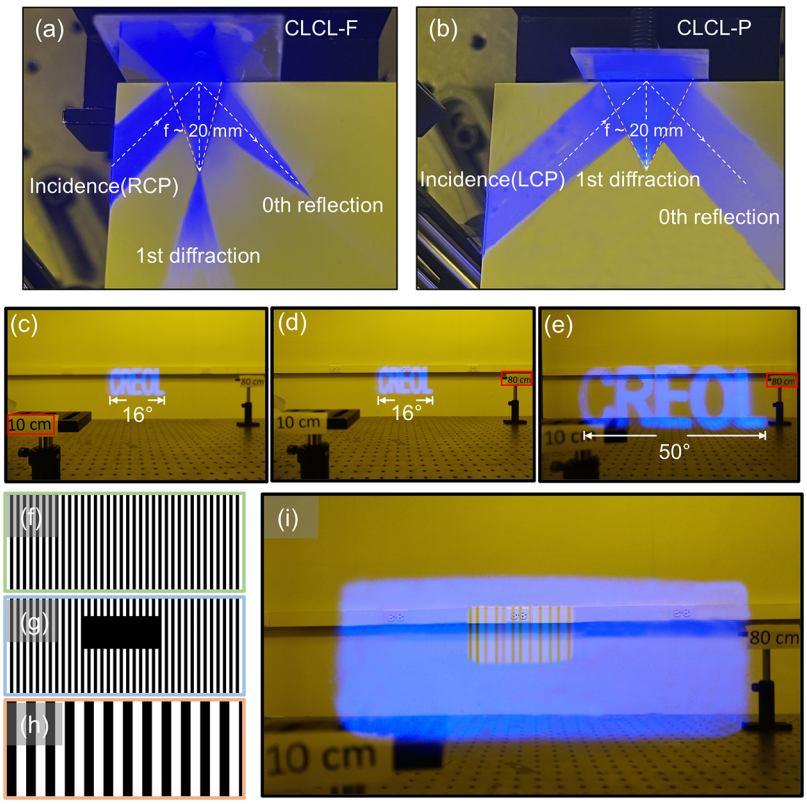

Figure 4. Photos of (a) CLCL-F and (b) CLCL-P diffracting light. The displayed image is always in focus no matter at (c) near or (d) far depths. The system shows (d) foveal FoV and (e) peripheral FoV for RCP and LCP incident light with the same content. The focus depth is indicated by the red box. (f) The test pattern for angular resolution evaluation. (g) Peripheral image. (h) Foveal image. (i) The combined experimental output.

reflection light is focused obeying the law of reflection, and the first-order diffraction beam also focuses to a different spot. When the handedness of incident light is flipped and the off-axis lens is replaced by CLCL-P, as shown Figure 4b, the beam after the PBL starts to diverge. The diffracted light focuses to the same spot as in Figure 4a but with a larger FoV. The light color in Figure 4 is oversaturated, and the reflected intensity is about 1 order of magnitude lower than the diffracted. The zeroth-order reflection can be further suppressed by coating an antireflection film on the glass substrate.

To prove the feasibility of the proposed Maxwellian foveated display, a benchtop demonstration was built, as illustrated in Figure 3d. A phone camera (One Plus 5T) was placed at 20 mm in front of the CLC lenses, and its shutter speed was set to 1/15 s. Two CLC lenses, responsible for peripheral and foveal FoV, respectively, were stacked together. The polarization of input light from the LBS (SONY, MP-CL1) was manually modulated by two orthogonal circular polarizers. A notch filter (Thorlabs, λ = 457 nm) was adopted to control the incident light wavelength and reduce its intensity. We chose a telephoto positive lens (f = 20 cm) as the collimation lens. Such a long focal length was adopted to exaggerate the display resolution enhancement effect. In practice, a condenser with an ultrashort focal length could be applied. For the LCP incident light, the collimated light was diverged by the PBL and converted to RCP light. Similarly, the collimated RCP light was converged by the PBL and converted to LCP light. To avoid image horizontal stretching due to off-axis projection from the light engine to the CLC lenses, as shown in Figure S1a,b, we horizontally shrink the input image for the LBS projector by a factor of cos θ, where θ is the off-axis angle indicated in Figure S1. Since the human visual system is very sensitive to the discontinuities in the observed images, blending techniques are required to smoothen the boundary between foveal and peripheral views. As pointed out by Kim et al.,[8] a linear blending algorithm can be applied to both foveal and peripheral images, where a Gaussian blur is applied to match the spatial frequency of two images for achieving a smoother transition.

The displayed image in a Maxwellian display should always stay in focus, regardless of the focal length of the combiner. To examine this characteristic, the incident light is modulated to RCP light. In Figure 4c,d, the focal length of the camera is adjusted to near (10 cm) and far (80 cm) depths, and the displayed images "CREOL" are in focus for both situations. When the incident light is switched to LCP light, a much larger FoV is shown in Figure 4e. The measured horizontal FoV is 16° for the foveal view and 50° for the peripheral view. This ratio (~3.12) agrees well with the 3.18× originally designed enhancement ratio. The image qualities of foveal and peripheral images can be evaluated by the modulation transfer function (MTF) of the imaging system. In an experiment, MTF can be determined by measuring the contrast ratio of bar patterns with different spatial frequencies. A monochrome 1951 USAF resolution target can be a good display pattern for such a measurement.

Although the full horizontal resolution of the LBS used in the experiment is 1920 pixels, the collimation lens with a long focal length allows us to only exploit a small portion of it. With fewer pixels, the image quality between two views can be intuitively evaluated. The actual pixel number implemented is 73(H) × 30(V). We designed a test pattern consisting of

https://doi.org/10.1021/acsaom.2c00203
ACS Appl. Opt. Mater. XXXX, XXX, XXX−XXX

alternating arranged black and white stripes with equally spaced at one pixel, as shown in Figure 4f. The corresponding peripheral image and foveal image is demonstrated in Figure 4g,h. The position of the foveal view is left empty in Figure 4g, and this part of image is enlarged ∼3× in Figure 4h accordingly. Since in the experiment we do not employ a switchable polarization rotator, the polarization state of the incident light is manually modulated by circular polarizers, without synchronization. As a result, the images of peripheral view and foveated view are taken separately by manually changing the displayed contents and incident polarization state, while keeping the camera still. We then crop the foveal region and replace the corresponding pixels in the peripheral image to obtain Figure 4i. We see that the stripes are fully indistinguishable in the peripheral view. Nevertheless, in the foveal view, the stripes can be clearly discerned, despite uneven thickness. The reasons can be 4-fold. First, the beam will diverge due to diffraction while propagating. If the beam size gets too large, the display fails to satisfy the resolving power of the human eye. Second, due to the raster scanning mechanism of the LBS, the perceived resolution is lower than the claimed parameters. Third, although the off-axis CLC lenses are fabricated to reconstruct a focused beam to the eye pupil without aberration, the employed collimation lens is not ideal. Fourth, there is still some misalignment in the demonstration, which cannot reproduce the setup during exposure. To enhance the image quality, an aspherical condenser could give a better plane-wave beam shaping. In addition, there is no need to squeeze out the maximum resolution of the LBS, since the theoretical maximum foveal angular resolution reaches 60 cpd, which is well beyond the human resolution limit. In addition, although the prototype only demonstrates a single eyebox and monochromatic images, this method is compatible with pupil-steering[27] and full-color AR displays by stacking multiple layers of CLC lenses.

CONCLUSION

In this paper, we propose and experimentally demonstrate a Maxwellian foveated AR display based on a single light engine by using a temporal polarization multiplexing method. The optical combiners are two polarization-selective CLC lenses and one PBL for separating the foveal and peripheral views. One CLC lens provides a large FoV, while the other realizes a high angular resolution imaging in a small fovea region. The angular resolution of the foveal view is enhanced by 3.12× compared to the peripheral while maintaining a compact form factor. By employing polarization-selective planar lenses, the setup of foveated AR displays becomes simpler due to the reduction in the number of panels and optical components, resulting in a more compact, lightweight, aberration-free, and easily integrated system. At the same time, the features of Maxwellian displays are preserved, making the system always-in-focus. This design could find promising applications in various mixed-reality display devices.

ASSOCIATED CONTENT

Supporting Information

The Supporting Information is available free of charge at https://pubs.acs.org/doi/10.1021/acsaom.2c00203.

Paraxial raytracing analysis of the foveated display system (PDF)

AUTHOR INFORMATION

Corresponding Author

Shin-Tson Wu − *College of Optics and Photonics, University of Central Florida, Orlando 32816 Florida, United States;* orcid.org/0000-0002-0943-0440; Phone: +1 (407) 823-4763; Email: swu@creol.ucf.edu

Authors

Qian Yang − *College of Optics and Photonics, University of Central Florida, Orlando 32816 Florida, United States*

Yannanqi Li − *College of Optics and Photonics, University of Central Florida, Orlando 32816 Florida, United States*

Yuqiang Ding − *College of Optics and Photonics, University of Central Florida, Orlando 32816 Florida, United States*

Complete contact information is available at: https://pubs.acs.org/10.1021/acsaom.2c00203

Author Contributions

Q.Y. and Y.L. contributed equally to this work.

Notes

The authors declare no competing financial interest.

ACKNOWLEDGMENTS

We are indebted to Goertek Electronics for the financial support.

REFERENCES

(1) Yin, K.; Hsiang, E. L.; Zou, J.; Li, Y.; Yang, Z.; Yang, Q.; Lai, P. C.; Lin, C. L.; Wu, S. T. Advanced Liquid Crystal Devices for Augmented Reality and Virtual Reality Displays: Principles and Applications. *Light: Sci. Appl.* **2022**, *11*, 161.

(2) Chang, C.; Bang, K.; Wetzstein, G.; Lee, B.; Gao, L. Toward the Next-Generation VR/AR Optics: A Review of Holographic near-Eye Displays from a Human-Centric Perspective. *Optica* **2020**, *7* (11), 1563−1578.

(3) Hsiang, E. L.; Yang, Z.; Yang, Q.; Lai, P. C.; Lin, C. L.; Wu, S. T. AR/VR Light Engines: Perspectives and Challenges. *Adv. Opt. Photon* **2022**, *14* (4), 783−861.

(4) Kramida, G. Resolving the Vergence-Accommodation Conflict in Head-Mounted Displays. *IEEE Transactions on Visualization and Computer Graphics* **2016**, *22* (7), 1912−1931.

(5) Li, Y.; Yang, Q.; Xiong, J.; Yin, K.; Wu, S. T. 3D Displays in Augmented and Virtual Realities with Holographic Optical Elements [Invited]. *Opt. Express* **2021**, *29* (26), 42696−42712.

(6) Hua, H. Enabling Focus Cues in Head-Mounted Displays. *Proceedings of the IEEE* **2017**, *105* (5), 805−824.

(7) Tan, G.; Lee, Y. H.; Zhan, T.; Yang, J.; Liu, S.; Zhao, D.; Wu, S. T. Foveated Imaging for Near-Eye Displays. *Opt. Express* **2018**, *26* (19), 25076−25085.

(8) Kim, J.; Jeong, Y.; Stengel, M.; Akşit, K.; Albert, R.; Boudaoud, B.; Greer, T.; Kim, J.; Lopes, W.; Majercik, Z.; Shirley, P.; Spjut, J.; McGuire, M.; Luebke, D. Foveated AR: Dynamically-Foveated Augmented Reality Display. *ACM Trans. Graph* **2019**, *38* (4), 99.

(9) Lee, S.; Wang, M.; Li, G.; Lu, L.; Sulai, Y.; Jang, C.; Silverstein, B. Foveated Near-Eye Display for Mixed Reality Using Liquid Crystal Photonics. *Sci. Rep* **2020**, *10*, 16127.

(10) Lyu, P.; Hua, H. Perceptual-Driven Approach to Statically Foveated Head-Mounted Displays. *Opt. Express* **2021**, *29* (21), 33890−33914.

(11) Yoo, C.; Xiong, J.; Moon, S.; Yoo, D.; Lee, C. K.; Wu, S. T.; Lee, B. Foveated Display System Based on a Doublet Geometric Phase Lens. *Opt. Express* **2020**, *28* (16), 23690−23702.

(12) Yin, K.; He, Z.; Li, Y.; Wu, S. T. Foveated Imaging by Polarization Multiplexing for Compact Near-eye Displays. *J. Soc. Inf. Disp* **2022**, *30* (5), 381−386.
(13) Xiong, J.; Li, Y.; Li, K.; Wu, S. T. Aberration-free Pupil Steering Maxwellian Display with Wide-view Broadband Polarization Converters. *J. Soc. Inf. Disp* **2021**, *29* (5), 298−304.
(14) Kobashi, J.; Yoshida, H.; Ozaki, M. Planar Optics with Patterned Chiral Liquid Crystals. *Nat. Photon* **2016**, *10*, 389−392.
(15) Chen, P.; Wei, B. Y.; Hu, W.; Lu, Y. Q. Liquid-Crystal-Mediated Geometric Phase: From Transmissive to Broadband Reflective Planar Optics. *Adv. Mater.* **2019**, *32*, 1903665.
(16) Li, Y.; Zhan, T.; Wu, S. T. Flat Cholesteric Liquid Crystal Polymeric Lens with Low F-Number. *Opt. Express* **2020**, *28* (4), 5875−5882.
(17) Chen, P.; Ma, L. L.; Hu, W.; Shen, Z. X.; Bisoyi, H. K.; Wu, S. B.; Ge, S. J.; Li, Q.; Lu, Y. Q. Chirality Invertible Superstructure Mediated Active Planar Optics. *Nat. Commun.* **2019**, *10*, 2518.
(18) Lee, Y. H.; Yin, K.; Wu, S. T. Reflective Polarization Volume Gratings for High Efficiency Waveguide-Coupling Augmented Reality Displays. *Opt. Express* **2017**, *25* (22), 27008−27014.
(19) Weng, Y.; Zhang, Y.; Cui, J.; Liu, A.; Shen, Z.; Li, X.; Wang, B. Liquid-Crystal-Based Polarization Volume Grating Applied for Full-Color Waveguide Displays. *Opt. Lett.* **2018**, *43* (23), 5773−5776.
(20) Kobashi, J.; Mohri, Y.; Yoshida, H.; Ozaki, M. Circularly-Polarized, Large-Angle Reflective Deflectors Based on Periodically Patterned Cholesteric Liquid Crystals. *Optical Data Processing and Storage* **2017**, *3* (1), 61−66.
(21) Xiong, J.; Yang, Q.; Li, Y.; Wu, S. T. Holo-Imprinting Polarization Optics with a Reflective Liquid Crystal Hologram Template. *Light Sci. Appl.* **2022**, *11*, 54.
(22) Nersisyan, S. R.; Tabiryan, N. V.; Steeves, D. M.; Kimball, B. R. Characterization of Optically Imprinted Polarization Gratings. *Appl. Opt.* **2009**, *48* (21), 4062−4067.
(23) Gu, Y.; Weng, Y.; Wei, R.; Shen, Z.; Wang, C.; Zhang, L.; Zhang, Y. Holographic Waveguide Display With Large Field of View and High Light Efficiency Based on Polarized Volume Holographic Grating. *IEEE Photonics Journal* **2022**, *14* (1), 7003707.
(24) Li, Y.; Yang, Q.; Xiong, J.; Li, K.; Wu, S. T. Dual-Depth Augmented Reality Display with Reflective Polarization-Dependent Lenses. *Opt. Express* **2021**, *29* (20), 31478−31487.
(25) Nys, I.; Stebryte, M.; Ussembayev, Y. Ye.; Beeckman, J.; Neyts, K. Tilted Chiral Liquid Crystal Gratings for Efficient Large-Angle Diffraction. *Adv. Opt. Mater.* **2019**, *7*, 1901364.
(26) Yin, K.; He, Z.; Wu, S. T. Reflective Polarization Volume Lens with Small F-Number and Large Diffraction Angle. *Adv. Opt. Mater.* **2020**, *8*, 2000170.
(27) Xiong, J.; Li, Y.; Li, K.; Wu, S. T. Aberration-Free Pupil Steerable Maxwellian Display for Augmented Reality with Cholesteric Liquid Crystal Holographic Lenses. *Opt. Lett.* **2021**, *46* (7), 1760−1763.

https://doi.org/10.1021/acsaom.2c00203
ACS Appl. Opt. Mater. XXXX, XXX, XXX−XXX